TiAl金属间化合物电子束焊接头应力场分布特征

陈国庆，　张秉刚，　刘　伟，　冯吉才*
(哈尔滨工业大学 现代焊接生产技术国家重点实验室，哈尔滨　150001)

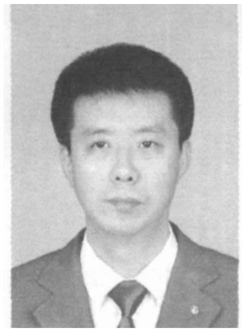

陈国庆

摘　要：采用热弹塑性有限元方法，对 TiAl金属间化合物平板电子束焊接接头的焊接应力进行了三维数值模拟，并分析了应力分布状态与裂纹特征之间的关系。结果表明，沿焊缝方向 σ_x为残余拉应力，在焊道中部维持在较高水平，最高拉应力为 390 MPa。焊道中部横截面 σ_x方向为残余拉应力，在热影响区附近达到最大值 415 MPa；σ_y方向也为残余拉应力，且在距焊缝中心 1.9 mm处达到最高值 160 MPa左右。在不同焊接热输入条件下接头最高抗拉强度为 304.7 MPa，断裂发生在接头热影响区附近，即残余应力最大的区域。

关键词：TiAl金属间化合物；电子束焊；应力场分布
中图分类号：TG456.3　文献标识码：A　文章编号：0253－360X(2010)01－0001－04

0　序　　言

TiAl金属间化合物具有金属的韧性，同时具有陶瓷的高温性能，因此在某些特殊需求的结构上获得应用[1,2]。有关 TiAl金属间化合物的性能特点及其应用前景已有大量报道，需要解决的主要问题是其连接性的改善。TiAl固相焊接性较好，但接头存在形式受限、叠加增重和使用温度相对较低等不足之处[3－5]。熔化焊方法可避免这些问题，但接头极易形成裂纹缺陷[6]。TiAl金属间化合物电子束焊接接头极易产生冷裂纹，原因在于 TiAl本身是一种典型的脆性材料，特定的焊接热循环更容易使接头组织脆硬化，变形能力及断裂韧性降低。然而除了组织因素外，焊接热循环对于裂纹的产生也有很大影响。电子束焊接特有的快速加热和冷却过程使接头处形成较大的热致应力，焊后冷却过程中当热致拉应力的幅值超过某一数值时就会致使接头开裂[7,8]。为此对 TiAl金属间化合物电子束焊接接头应力场分布特征进行研究，通过有限元数值模拟分析接头焊接应力分布规律，探讨残余应力对接头性能的影响，研究热致应力对裂纹形成的作用，从而为改善 TiAl金属间化合物电子束焊接性提供理论依据。

收稿日期：2009－09－11
基金项目：哈尔滨工业大学优秀青年教师培养计划资助项目（HITQNJS.2008.015）；黑龙江省杰出青年科学基金资助项目（2004）
*参加此项研究工作的还有刘玉龙

1　有限元模型建立

数值模拟采用非线性有限元 Marc2000程序，焊接过程为平板对接电子束焊。试件尺寸为 60 mm×30 mm×2.5 mm，焊接试件如图 1所示。

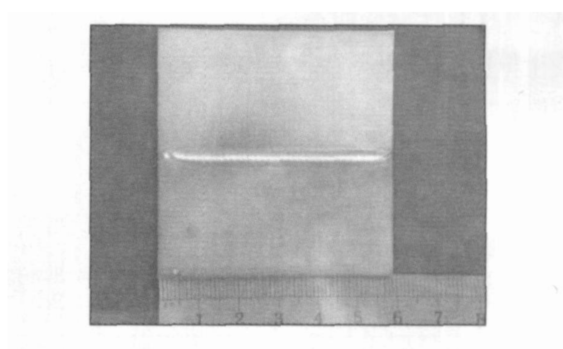

图 1　TiAl电子束焊接实际构件
Fig.1　Photo of TiAl join structure

1.1　网格划分

电子束焊接焦点附近束斑直径很小，在焊接过程中只有局部区域材料达到熔化和气化温度，而远离焊缝的母材区域温度较低。

为保证数值模拟的计算精度，同时节省计算时间，计算时采用非均匀网格划分。在热源作用的区域加大计算精度，采用细网格划分，而在远离焊缝处采用粗网格划分，以便提高计算精度和计算速度，网格划分如图 2所示。

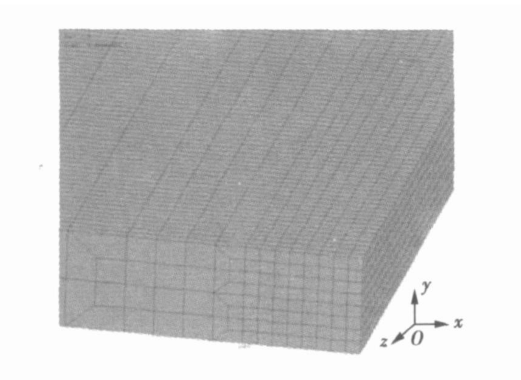

图 2 TiAl计算采用的有限元网格模型
Fig. 2 Finite element model of TiAl calculation

1.2 热源模型

电子束焊接时熔池的形成过程存在匙孔效应，依据熔池和匙孔对能量吸收和再分布的影响，采用双椭球体热源模型，将熔池分成前后两个部分，该热源模型的能量密度分布为

$$q(x,y,z)=\frac{6\sqrt{3}Q}{abc\pi^{3/2}}\exp\left(-3x^2/a^2\right)\exp\left(-3y^2/b^2\right)\exp\{-[z+v(\tau-t)]^2/c^2\} \quad (1)$$

式中：Q为电子束功率；c为能量分布参数，表示95%的入射能流集中在以其为半径的圆形区域内；v，t分别为焊接速度和时间.

1.3 材料参数

TiAl的热物理性能参数受热循环温度的影响，计算中采用随温度变化的物性参数，如表 1所示. 其中弹性模量、屈服强度、线膨胀系数和导热系数的高温数据采用线性回归法进行外推. TiAl金属间化合物的泊松比几乎不随温度变化，取值为 0.22.

表 1 TiAl在不同温度时的热物理参数
Table 1 Thermal physical parameters of TiAl at different temperatures

温度 T/℃	弹性模量 E/GPa	屈服强度 R_{eL}/MPa	线胀系数 $\alpha_l/10^{-6}K^{-1}$	导热系数 λ/ ($W\cdot m^{-1}\cdot K^{-1}$)	比热容 c/ ($J\cdot kg^{-1}\cdot K^{-1}$)
25	172.0	395.9	11.0	12.0	400
150	166.5	373.7	11.7	14.0	430
300	162.0	358.9	12.3	15.0	465
450	157.5	336.7	13.2	17.5	500
600	153.0	329.3	14.0	21.0	520
900	144.0	259.0	15.0	24.0	600

2 计算结果及分析

2.1 沿焊缝方向三向应力分布

电子束焊接时，随电子束热源移入，试件待焊部位温度急剧上升，当等效应力大于 TiAl金属间化合物的屈服强度时，接头局部就会产生塑性变形. 随热源的移出，焊缝及其周围区域温度迅速下降，金属开始恢复弹性，此时的应力状态由塑性转变为弹性状态. 随着温度的进一步降低，接头恢复刚性后无法继续通过变形释放应力，从而在接头处形成较大的残余应力. 图 3为 TiAl电子束焊后接头残余应力的分布状态图，其中箭头所指为焊接方向. 由图 3可见，焊缝及其周围区域为残余拉应力，远端母材为残余压应力.

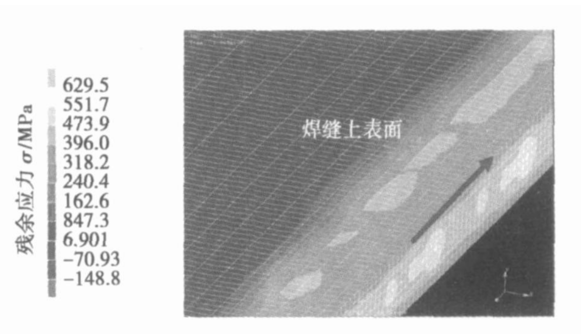

图 3 接头残余应力分布图
Fig. 3 Residual stress distribution of joints

由图 3可见，焊缝中心的残余应力最大，接头冷却到室温时沿焊缝方向上表面三向应力分布如图 4所示. 由图 4可见，σ_x方向为残余拉应力，且在沿焊缝方向中部达到较高水平，最高拉应力为 390 MPa. σ_y方向为残余压应力，在沿焊缝中部幅值较小，约为 80 MPa，仅在焊缝的起焊处和终焊处压应力值较高，最大残余压应力为 406 MPa. 由于是薄板焊接，因此 σ_z方向残余应力整体较小.

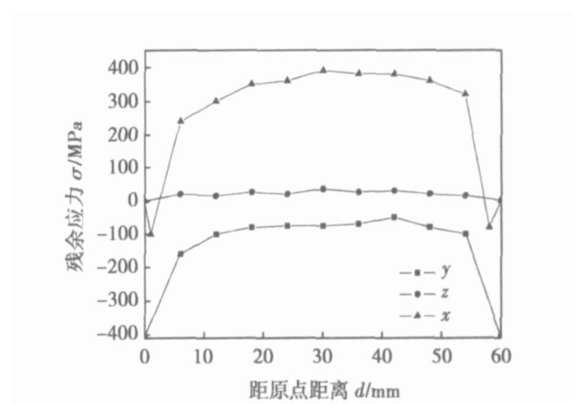

图 4 接头沿焊缝方向三向应力分布
Fig. 4 Three dimensional stress distribution of joints along welding direction

由上述模拟结果可知，TiAl金属间化合物薄板电子束焊接接头冷却到恢复刚性之后，对接头具有

破坏作用的残余拉应力主要分布在 σ_x 方向上,即沿焊缝方向承受了较大的残余拉应力. 实际焊接时当残余拉应力的幅值超过某一极限值时接头产生冷裂纹,且裂纹方向整体垂直于焊缝,如图 5所示,箭头所指为垂直于焊缝方向上的裂纹.

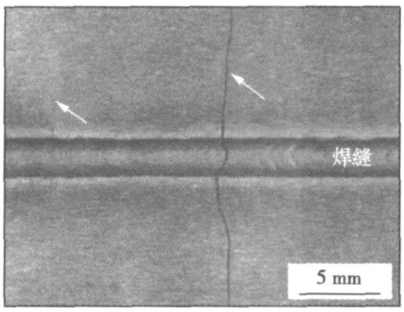

图 5　接头裂纹垂直于焊缝分布特征
Fig. 5　Crack distribution character of joints

2.2　垂直于焊缝方向三向应力分布特征

图 6为焊后冷却到室温时焊道中部横截面上残余应力的分布状态云图. 可见接头横截面上应力状态比较复杂,主要为残余压应力,分布在焊道的上下表面处,这种残余压应力分布特征对接头避免焊后开裂是有益的.

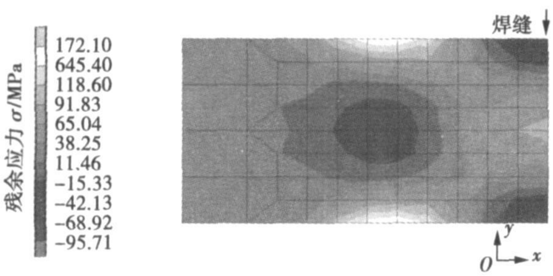

图 6　接头横截面残余应力分布云图
Fig. 6　Residual stress distribution along cross-section of joints

图 7为焊道中部横截面三向残余应力分布,由图 7可见,距焊缝中心一定距离处残余应力最大. 其中 σ_x方向为残余拉应力,在热影响区处达到最大值 415 MPa,随距焊缝距离增大拉应力迅速衰减,在母材区域表现为幅值较小且稳定的残余压应力. σ_y方向残余应力分布在距焊缝中心 1.9 mm处,即热影响区处达到最大值,其幅值为 160 MPa左右,某些情况下该残余应力会使接头沿焊缝方向开裂,开裂位置分布在热影响区附近,实际焊接开裂如图 8所示. σ_z方向由于是薄板焊接拘束较小,表现出较小的残余应力.

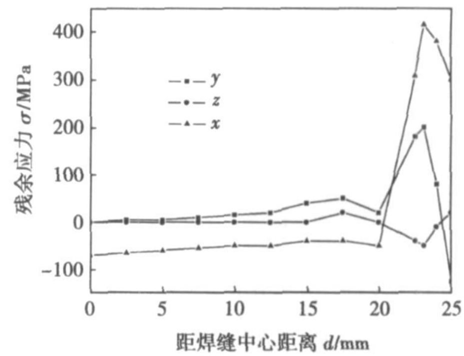

图 7　接头横截面三向残余应力分布
Fig. 7　Three dimensional residual stress distribution of joints along cross-section

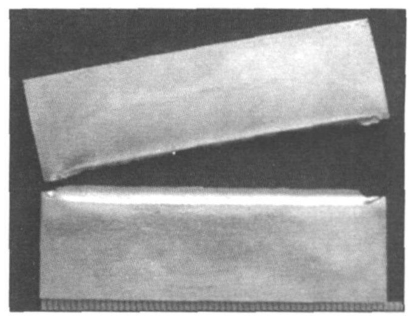

图 8　沿焊缝方向整体开裂试件
Fig. 8　Workpiece with cracks along welding direction

3　试验验证

为验证数值模拟的结果,对不同焊接热输入时所获电子束焊接接头进行了抗拉强度试验,结果如图 9所示. 在文中试验范围内所获接头最高抗拉强度为 304.7 MPa. 该强度值低于有限元模拟结果中

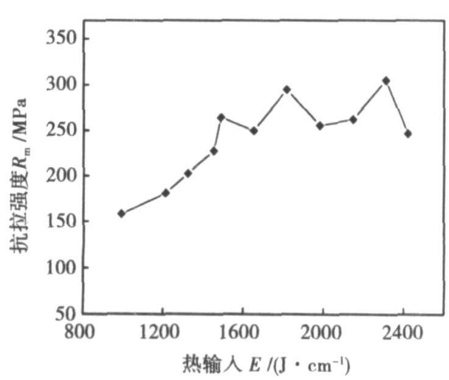

图 9　焊接热输入对接头抗拉强度的影响
Fig. 9　Influence of heat input on tensile strength

的残余应力值,因此接头在焊后产生裂纹缺陷.图 10显示了拉伸断裂发生在接头热影响区附近,这与模拟结果一致.

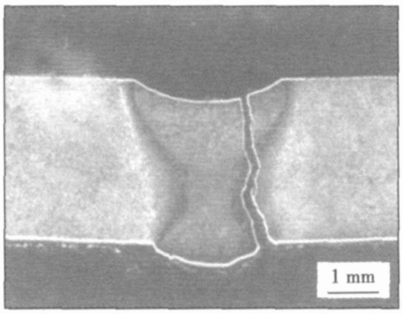

图 10 接头的断裂路径
Fig. 10 Fracture path of weld joints

4 结 论

(1)模拟了 TiAl电子束焊接接头残余应力场分布特征. 沿焊缝方向 σ_x为残余拉应力,在焊道中部维持在较高水平,最高拉应力为 390 MPa. σ_y方向为幅值较小的残余压应力.

(2)焊道中部横截面 σ_x方向为残余拉应力,在热影响区附近达到最大值 415 MPa, σ_y方向也为残余拉应力,且在距焊缝中心 1. 9 mm处最高值为 160 MPa左右, σ_z方向表现出较小的残余应力.

(3)对模拟结果进行试验验证,在不同焊接热输入条件下接头最高抗拉强度为 304. 7 MPa,断裂发生在接头热影响区附近,即模拟中残余应力最大区域,说明模拟结果基本正确.

参考文献:

[1] Saari H, Beddoes J, Seo D Y, et al. Development of directionally solidified γ-TiAl structures[J]. Intermetallics, 2005(13): 937—943.
[2] Dlouhy A, Kucharova K. Creep and microstructure of near-gamma TiAl alloys[J]. Intermetallics, 2004(12): 705—711.
[3] Shiue R K, Wu S K, Chen S Y. Infrared brazing of TiAl intermetallic using bag-8 braze alloy[J]. Acta Materialia, 2003(51): 1991—2004.
[4] Cam G, Kocak M. Diffusion bonding of investment cast γ-TiAl[J]. Journal of Materials Science, 1999(34): 3345—3354.
[5] 吴国清, 阮中健, 黄 正. γ-TiAl基合金的表面激光处理及超塑性扩散连接[J]. 中国有色金属学报, 2001, 11(5): 760~763.
Wu Guoqing, Ruan Zhongjian, Huang Zheng. Superplastic forming and diffusion bonding of laser surface melted TiAl intermetallic alloy[J]. The Chinese Journal of Nonferrous Metals, 2001, 11(5): 760—763.
[6] Arenas M F, Acoff V L. The effect of postweld heat treatment on gas tungsten arc welded gamma titanium aluminide[J]. Scripta Materialia, 2002, 46: 241—246.
[7] 周 琦, 刘方军, 关 桥. 电子束流的动态焦点和深穿极值效应[J]. 焊接学报, 2004, 25(4): 19—22.
Zhou Qi, Liu Fangjun, Guan Qiao. Dynamic focal spot and extremum effect of deep penetration of electron beam[J]. Transactions of the China Welding Institution, 2004, 25(4): 19—22.
[8] 李卓然, 曹 健, 冯吉才. TiB2金属陶瓷/TiAl钎焊连接接头应力的数值模拟[J]. 焊接学报, 2003, 24(3): 1—4.
Li Zhuoran, Cao Jian, Feng Jicai. FEM analysis of thermal/residual stresses in brazing TiB—2 cermet/TiAl joints[J]. Transactions of the China Welding Institution, 2003, 24(3): 1—4.

作者简介: 陈国庆, 男, 1972年出生, 博士研究生, 讲师. 研究方向为新材料及异种材料电子束焊接. 发表论文 10余篇.
Email: chenguoqing@hit.edu.cn

MAIN TOPICS, ABSTRACTS & KEY WORDS

Distributive characteristic of stress field in electron beam welded joint of TiAl intermetalics plates CHEN Guoqing, ZHANG Binggang, LIU Wei, FENG Jicai, LIU Yulong (National Key Laboratory of Advanced Welding Production Technology, Harbin Institute of Technology, Harbin 150001, China). p 1-4

Abstract: Welding stress in electron beam welding joint of TiAl intermetalics plates, as well as the relationship between stress distribution and crack characteristic were numerical stimulated using thermo-elastic-plastic finite element method. The results showed that stress σ_x along welding direction was tensile stress, and which was a relatively high level in central weld. With the highest value of 390 MPa, σ_x in the cross section in central weld was tensile stress and it came to the largest value of 415 MPa in HAZ. In the same section, σ_y perpendicular to welding direction was also tensile stress and the largest value was approximately to 160 MPa at the site 1.9 mm away from weld center line. The highest tensile strength of the joints welded under different heat inputs was 304.7 MPa. Fracture occured near HAZ, e.g. the place where the residul stress value was the largest from the numerical simulation results.

Key words: TiAl intermetalics plates; electron beam welding; stress field distribution

Microstructure and hardness of laser welded joint of China low activation martensitic steel LEI Yucheng, HAN Mingjuan, ZHU Qiang, JU Xin[2] (1. School of Material Science and Engineering of Jiangsu University, Zhenjiang 212013, Jiangsu, China; 2. Physics Department, University of Science and Technology of Beijing, Beijing 100083, China). p 5-8

Abstract: Laser welding of 6mm-thick CLAM is conducted with different welding parameters by 4 kW Nd:YAG. Microstructure and hardness of welded joint are analyzed with pre- and post tempering respectively. The results show that the microstructure of welded joints are mainly coarse lath martensite and hardness of welded joint is increased as welding speed rises before tempering. After tempering, microstructure of welded joint is tempered lath martensite. A large amount of carbide particles are observed in original austenite grain boundary and martensite lath by SEM, which lead to a slight increase in the hardness of weld zone to base metal relatively. HAZ is not softened.

Key words: low activation martensitic steel; CLAM; YAG laser welding; microstructure; hardness

Analysis on mechanism of laser-assisted TIG arc ignition XIA Yuan, SONG Yonglun, RAN Guowei, SHI Linan (Department of Mechanical Engineering & Applied Electronics Technology, Beijing University of Technology, Beijing 100124, China). p 9-11, 16

Abstract: Laser-assisted TIG arc ignition was applied by 1000W semiconductor laser. Using emission spectroscopy method, the arc ignition process of the spectral information at different moments was observed, while the transient characteristics of electron density were obtained by Stark broadening method. The results show that, in the arc ignition process, the contribution of electron from different elements is obviously different. In the beginning of arc ignition, the contribution of electron was from the ionizing metallic element, as time increasing, the contribution of electron from gas was gradually increased, and for the existence of the electric field between electrodes, high-temperature gas quickly formed a cascade of ionizing and finally arc was established.

Key words: laser; TIG arc; arc ignition; spectral diagnosis; mechanism

H_2S stress corrosion invertigation of pipeline steel welded joints XU Lianyong[1,2], JING Hongyang[1,2], CAO Jun[3], LI Chunguo, SUN Youhui[3] (1. School of Materials Science and Engineering, Tianjin University, Tianjin 300072, China; 2. Tianjin Key Laboratory of Advanced Joining Technology, Tianjin 300072, China; 3. Offshore Oil Engineering Co. Ltd, Tianjin 300452, China). p 12-16

Abstract: The H_2S stress corrosion tests were conducted for the welded joints of X56 steel and X65 steel under various welding processes in order to investigate the susceptibility of weld metal and heat-affected zone (HAZ) to H_2S stress corrosion cracking (SCC), and the wedge-opening loading (WOL) specimens were used in the tests. The test results showed that small crack growth occurred in all specimens, and the crack stopped to grow when the stress intensity factor K reached the critical value (threshold stress intensity factor). In this paper, the H_2S stress corrosion resistance of HAZ was better than that of weld metal for the welded joints of X56 and X65 steel. In addition, the corrosion resistance of HAZ and weld metal were worse than that of base metal inferred to literature, which was caused by grain growth coarsening, welding residual stress of HAZ and weld metal, weld strength overmatching and welding defects.

Key words: stress corrosion; welded joint; pipeline steel; critical stress intensity factor

Molecular dynamics simulations of interface interactions of POSS in lead free solder joints ZENG Fanlin[1], SUN Yi[1], ZHOU Yu[2], LI Qingkun[2] (1. Department of Astronautic Science and Mechanics, Harbin Institute of Technology, Harbin 150001, China; 2. Material Science and Engineering, Harbin Institute of Technology, Harbin 150001, China). p 17-20

Abstract: The interface interactions of cyclohexenyl-